LRP 714/01 November 2001

The Effect of the Feedback Controller on Superconducting Tokamak AC Losses + AC-CRPP user manual

B. Schärz, P. Bruzzone, J.-Y. Favez,
J.B. Lister & E. Zapretilina

CRPP
Centre de Recherches en Physique des Plasmas
Association Euratom - Confédération Suisse

ÉCOLE POLYTECHNIQUE
FÉDÉRALE DE LAUSANNE

Centre de Recherches en Physique des Plasmas (CRPP)
Association Euratom - Confédération Suisse
Ecole Polytechnique Fédérale de Lausanne
PPB, CH-1015 Lausanne, Switzerland
phone: +41 21 693 34 82 / 87 — fax +41 21 693 51 76

Centre de Recherches en Physique des Plasmas
Technologie de la Fusion (CRPP-TF)
Association Euratom - Confédération Suisse
Ecole Polytechnique Fédérale de Lausanne
CH-5232 Villigen-PSI, Switzerland
phone: +41 56 310 32 59 — fax +41 56 310 37 29

http://crppwww.epfl.ch/

LRP 714/01 November 2001

The Effect of the Feedback Controller on Superconducting Tokamak AC Losses + AC-CRPP user manual

B. Schärz, P. Bruzzone, J.-Y. Favez,
J.B. Lister & E. Zapretilina

ISSN 0458-5895

The Effect of the Feedback Controller on Superconducting Tokamak AC Losses

Beat Schärz[a] Pierluigi Bruzzone[b] Jean-Yves Favez[c]
Jonathan B. Lister*,[a] Elena Zapretilina[d]

November 22, 2001

*Corresponding author. Tel.: +41-21-693-3405; Fax.: +41-21-693-5176; E-mail: jo.lister@epfl.ch
[a]EPFL-CRPP, 1015 Lausanne, Switzerland
[b]EPFL-CRPP Fusion Technology, 5232 Villigen-PSI, Switzerland
[c]EPFL-DGM-IA, 1015 Lausanne, Switzerland
[d]Efremov Institute, St. Petersburg, Russian Federation

Abstract

Superconducting coils in a Tokamak are subject to AC losses when the field transverse to the coil current varies. A simple model to evaluate the AC losses has been derived and benchmarked against a complete model used in the ITER design procedure. The influence of the feedback control strategy on the AC losses is examined using this model. An improved controller is proposed, based on this study.

1 Introduction

Most present tokamaks use copper conductors for the creation of the magnetic fields required to provide the plasma equilibrium and to control the shape and position of the plasma cross section. Exceptions are Tore Supra, T-7 and T-15 which have superconducting toroidal field coils, the small tokamak TRIAM which has superconducting toroidal and poloidal field coils and the LHD Stellarators. These tokamaks operate with circular cross section plasmas and do not require active control of the vertical positional instability which is a property of vertically elongated plasma cross-sections.

The fusion power in a tokamak reactor plasma is less than the Ohmic power dissipated in copper poloidal and toroidal field coils, requiring superconducting magnets in any large device. The next generation of tokamaks under construction, K-STAR, SST-1 and HT-7U will require vertical position and active shape control and will be fully superconducting. The future large tokamak ITER is also naturally designed with superconducting coils. The interplay between the superconducting magnets and the plasma shape and position control will become important for these devices and presents one of their new features.

When the transverse field in superconducting magnets changes, the magnet generates two types of heat loss, the so-called coupling loss and the so-called hysteresis loss, grouped together as AC losses and described in Section 2 of this paper. The field variations which lead to losses are produced by the evolution of the equilibrium through the discharge, referred to as the scenario loss, and the action of the plasma position and shape controller, reffered to as feedback losses. During the design of ITER, studies were performed to estimate the effect of the action of the feedback control loops on the accumulated AC losses to determine the required cryogenic plant load and the local cooling requirements of the magnets. These estimates were performed with a code which analyzed the results of simulations of the plasma shape and position feedback control loops. The effect of the design of the controller on the AC losses has not yet been investigated.

The aim of this present paper is to determine to what extent the accumulated AC losses in ITER could be reduced by taking into account the losses themselves when designing the feedback control loops. In order to do this, a simple model of the AC losses, "AC-CRPP", had to be developed and is described in Section 2. At present, the AC losses are only calculated for the PF coils. This model was compared with all the detailed simulations available, in order to validate it. The action of the feedback control was simulated using a standard linearized model of the ITER tokamak [1] and using the standard ITER position and shape feedback controller [2], described in Section 3. In order to evaluate the feedback controller performance, a set of standard perturbations was used, corresponding to the ITER design methodology [3] and summarized in Section 3.

In Section 4, the results of these simulations are presented, showing that the basic calculations of the detailed code [4] agrees well enough with the AC-CRPP model to have confidence in using the AC-CRPP model to refine the feedback controller. The distribution of the AC losses among the different coils is also discussed in Section 5.

These results allowed us to modify the feedback controller, especially the fast part which guarantees the vertical stability, showing that the hysteresis

loss is only weakly affected by the controller design but that the coupling loss can be significantly reduced. A modified controller is proposed, to illustrate potential reductions using different design criteria.

In Section 6, we discuss the significance of these results for ITER, showing that the total AC losses are weakly dependent on controller design for the short 430 second flat-top, but that for longer pulse operation the AC losses could be usefully reduced by the approach presented.

2 AC Loss Model and Validation

2.1 Superconductors and AC Losses

2.1.1 Characterization of superconductors

Below a certain critical temperature T_c, superconductors lose their electrical resistivity. Superconductors show the *Meissner-Ochsenfeld-effect* (diamagnetic behavior) which is the expulsion of all external magnetic fields from their interior. The interior includes all the the material except for a very thin layer on the surface of the conductor (the London penetration depth λ). Inside this very thin surface layer an induced shielding current circulates, whose magnetic field compensates the external magnetic field.

Type I superconductors show a complete Meissner effect and expel all of the magnetic field from their interior up until a critical magnetic field B_c when they abruptly cease to behave like superconductors.

Type II superconductors only exhibit a partial Meissner effect except for weak magnetic fields up to a strength of B_{c1}, above they show progressively less expulsion until at a certain level of magnetic field B_{c2} they abruptly cease to behave as superconductors.

There is also a critical current density J_c above which the material loses superconductivity. T_c, B_c and J_c are interrelated.

Although there is no resistivity in superconducting cables, there are still AC losses in the presence of time-varying magnetic fields. The two most important types are hysteresis loss and coupling loss. They produce heat and are therefore important factors when designing the cryogenic system. Their relative importance depends on the application.

2.1.2 Hysteresis Loss

In Fig. 1 we illustrate a DC magnetization curve for a type II superconductor, of the type proposed for ITER. When a magnetic field is initially applied, the superconductor shows perfect diamagnetism, the shielding currents induced at the filament surface preventing the flux from penetrating ($M = -H$) up until B_{c1}. Above B_{c1} the flux gradually penetrates into the filament until it reaches its center at the first penetration field B_{p1}. For higher B the magnetization decreases and eventually becomes 0 at the upper critical field B_{c2} (upper branch). When the field is decreased, the average magnetization is > 0 (lower branch). The flux trapped at $B = 0$ is the residual magnetization.

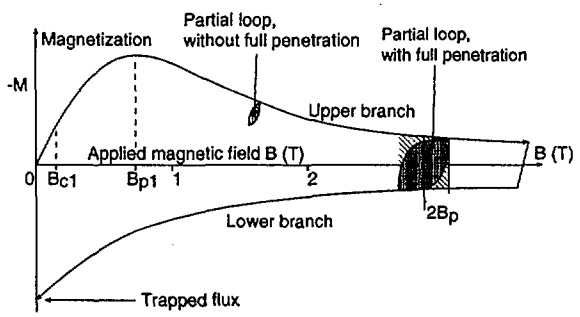

Figure 1: Magnetization vs. applied magnetic field for a type II superconductor.

If the external magnetic field is reversed after the initial magnetization, there has to be a certain field difference until the field reversal reaches the center of the conductor. Fig. 2 (a) shows the initial flux profile (dashed line) and the flux profile after a field reversal of $2B_p$ (solid line). B_p is the penetration field and is the difference between the external field and the field at the electrical center line of the conductor. To fully reverse the flux profile, a field change of $2B_p$ is needed. Fig. 1 includes a loop with full penetration. The shaded area between the demagnetization and magnetization path is the loss caused during the cycle. If the field difference is smaller, there is not full penetration and the resulting flux profile is shown in Fig. 2 (b).

It is assumed that the critical current density J_c is constant over the filament cross-section, so the flux profiles have a linear behavior and Bean's model [5] can be used, in which for a cylinder of diameter d_f and with an external magnetic field perpendicular to the cylinder axis,

$$B_{p\perp} = \frac{\mu_0 j_{c\parallel}(B) d_f}{\pi}. \tag{1}$$

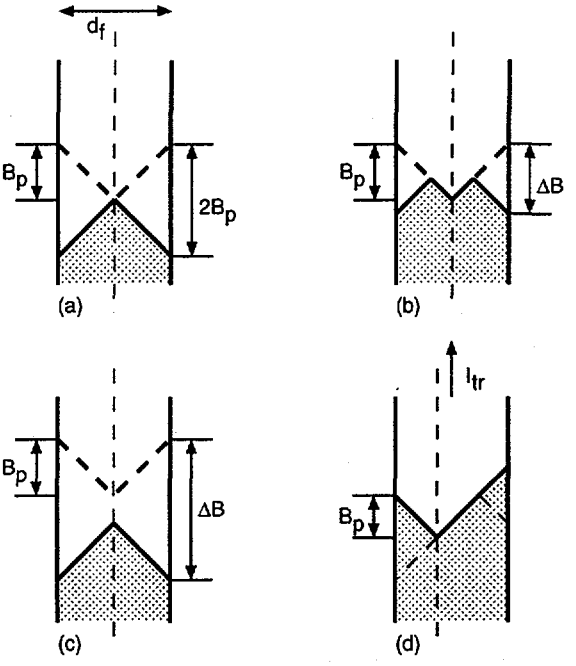

Figure 2: Penetration field without and with transport current. The solid profile represents the situation on the upper branch of the magnetization curve. The dashed profile represents the lower branch.

where $j_{c\|}$ is the critical current density of the superconductor, a function of temperature and external magnetic field, that can be obtained from measurements.

For closed cycles of magnetization and demagnetization, the energy loss q_h per unit volume of superconducting material is written as the integral of the magnetization M versus the applied magnetic field B with M the average value of magnetization,

$$q_h = \oint M(B)\,\mathrm{d}B \qquad (\mathrm{J/m^3}). \tag{2}$$

The hysteresis losses are independent of the field rate of change in time.

There are three simple cases, shown in Fig. 1 and Fig. 2:
For $\Delta B < 2B_{p\perp}$ (partial loop without full penetration):

$$q_{h,\perp} = \frac{\Delta B^3}{3\mu_0 B_{p\perp}}\left(1 - \frac{\Delta B}{4B_{p\perp}}\right) \qquad (\mathrm{J/m^3}) \tag{3}$$

For $\Delta B > 2B_{p\perp}$ (partial loop with full penetration):

$$q_{h,\perp} = \frac{4}{3}\frac{B_{p\perp}^2}{\mu_0}\left(\frac{\Delta B}{B_{p\perp}} - 1\right) \qquad (\mathrm{J/m^3}) \qquad (4)$$

For $\Delta B \gg 2B_{p\perp}$ (partial loop with full penetration, approximation for large ΔB)

$$q_{h,\perp} \approx \frac{4}{3}\frac{B_{p\perp}\Delta B}{\mu_0} \qquad (\mathrm{J/m^3}) \qquad (5)$$

Hysteresis losses are calculated over a closed cycle of external magnetic field and are given per unit volume of superconductor (Joule/m^3).

The three cases are illustrated in Fig. 1. From the figure, the third case (light shaded area) overestimates the actual hysteresis loss.

If a longitudinal transport current I_{tr} is superimposed on the transverse field magnetization currents in a superconducting cylinder, the electric center line is moved from the geometric center to the periphery of the filament (Fig. 2 d). The flux profile is asymmetric and the penetration field decreases by a factor $(1-k)$:

$$k = \frac{I_{tr}}{I_{c\parallel}}, \qquad B_{p\perp}^k = B_{p\perp}(1-k) \qquad (\mathrm{T}) \qquad (6)$$

This also modifies the range of validity of Eq. 3 and Eq. 4 ($B_{p\perp}$ has to be replaced by $B_{p\perp}^k$). In addition, Eq. 5 is modified to:

$$q_{h,\perp} \approx \frac{4}{3}\frac{B_{p\perp}\Delta B}{\mu_0}(1+k^2) \qquad (\mathrm{J/m^3}). \qquad (7)$$

These assumptions are used to estimate the hysteresis loss in the AC-CRPP model. For further informations on hysteresis losses refer to [6].

2.1.3 Coupling Current Loss

Superconducting cables used in industrial applications are composed of several bundled strands, each containing thousands of filaments. The reason for this is to avoid flux jumps that can occur in cables with large filament diameters and to reduce hysteresis loss. The downside is the occurrence of a new class of losses, called coupling current losses, because of the magnetic coupling of strands and filaments in the presence of a time varying transverse magnetic field.

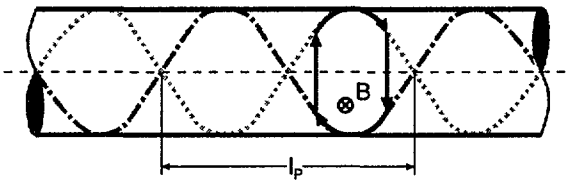

Figure 3: Look inside a strand with two twisted filaments embedded in a non-superconducting matrix. The arrows illustrate a current loop caused by the varying transverse magnetic field. The twist pitch l_p is an average value and caracterizes the length of a typical loop.

Two strands or filaments form an induction loop, in which the two superconducting parts are linked by two non-superconducting volumes. The induced loop current has to pass through this resistive area and thereby produces an ohmic loss. A time constant can be assigned to such a loop, which allows linking the field rate to the generated loss. This time constant for a twisted, multifilamentary composite can be expressed as

$$\tau = \frac{\mu_0 l_p^2}{8\pi^2 \rho} \qquad \text{(s)}. \tag{8}$$

which is the ratio of the loop inductance to the loop resistance, a function of the twist pitch l_p and the matrix resistivity ρ.

A multistage cable has a multitude of different loops and time constants τ_i. An overall time constant has to be used for coupling loss calculations, expressed as

$$n\tau = \sum_i n_i \tau_i \qquad \text{(s)}. \tag{9}$$

Due to the uncertitude in the resistance of the different loops, it is not reliable to estimate the time constant directly from the conductor geometrical data, so it has to be measured.

For a linear ramp of the transverse field, the coupling loss per unit volume of strand material is:

$$p_c = \frac{n\tau}{\mu_0} \dot{B}^2 \qquad \text{(W/m}^3\text{)} \tag{10}$$

and the loss per cycle is:

$$q_c = \frac{2n\tau}{\mu_0} \dot{B} \Delta B \qquad \text{(J/cycle/m}^3\text{)} \tag{11}$$

The coupling loss increases with the square of the field rate of change and would eventually become larger than the magnetic field energy density $\frac{1}{2}HB$. This is not possible and we observe that at high frequencies, the coupling currents cannot penetrate completely into the conductor, reducing the loss power.

If the duration of the ramp t_0 is smaller than 10τ the steady state formula overestimates the coupling loss by $\approx 10\%$. For faster ramps, the steady state formulas should be replaced by transient formulas.

For further informations on coupling current losses refer to [7]. Scaling laws for the critical properties of NbTi can be found in [8].

2.1.4 ITER Magnet Cables

The conductors to be used for the ITER PF coils are made out of 864, 1080 or 1440 strands with different winding schemes. The strands are composed of sub-elements and the actual superconducting filaments are between $5\,\mu$m and $7\,\mu$m, embedded in a copper matrix. These strands are surrounded by a steel jacket to absorb the high mechanical forces, Fig. 4

The central hole is a metal helix that carries most of the forced flow supercritical helium. At the inlet, the coolant is at 4.5 K and reaches a temperature of up to 5.5 K at the outlet, leaving a margin of $1 - 2$ K to the current sharing temperature.

The time between inlet and outlet is long in comparison with all loss mechanisms, so the coolant temperature can be considered as an integrator of the loss history during the time inside the conductor. The conductor is designed with enough margin to absorb all likely losses. The possible reduction could allow to downsize the superconducting cross section in the cables, reducing the overall cost.

Currently used filament diameters are around $7\,\mu$m and could be as low as $5\,\mu$m for the ITER coils. To reduce the conductor cost, it would be interesting to increase the filament diameter to at least $10\,\mu$m, allowing a potentially simpler and cheaper manufacturing process.

Other loss sources include conduction, thermal and nuclear radiation. The non-superconducting joints also generate losses due to ohmic heating. For ITER, the cryogenic system will have approximately 150 kW cooling power.

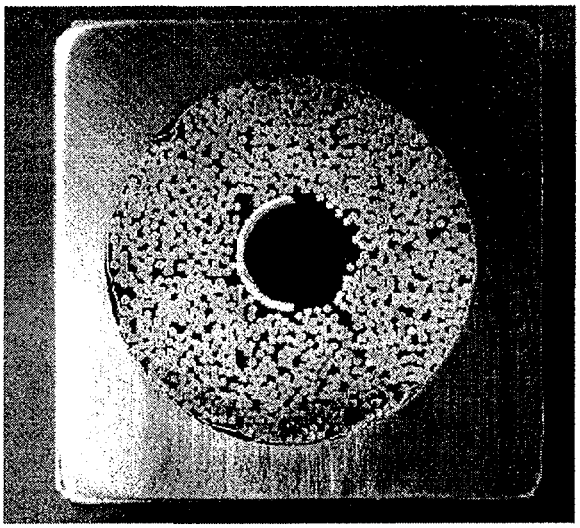

Figure 4: Cable-in-conduit (CICC) superconductor developed for the ITER Tokamak

2.2 Evaluation Method and AC-CRPP Model

2.2.1 Magnetic field evaluation

The AC losses in the PF coils are a function of the transverse magnetic field and its time derivative at the center of every turn. Sources of the transverse magnetic field are the toroidal currents in the PF and CS coils, the plasma and the conducting vacuum vessel. These sources are modeled as discrete sets of stationary current carrying loops, illustrated in Fig. 5 where the crosses represent the loops that model the coils, the circles represent the loops that model the vessel and the dots represent the loops that model the plasma. Simulations have shown that the influence of plasma position variations is small, so the plasma is assumed to be stationary. The TF coils also contribute to the transverse field because their field is not uniform along the perimeter, but this influence is small and therefore neglected in the model. The TF coil current itself is constant.

The loops representing the PF coil currents are distributed uniformly over the whole area of each PF coil and the PF coil current is the sum of the nominal equilibrium current plus the transient variations due to the action of the shape and position feedback controller. The vessel is modeled as a set of 56 loops that are identical to the states of the ITER state-space model used for control purposes. The plasma is modeled as a grid of loops that

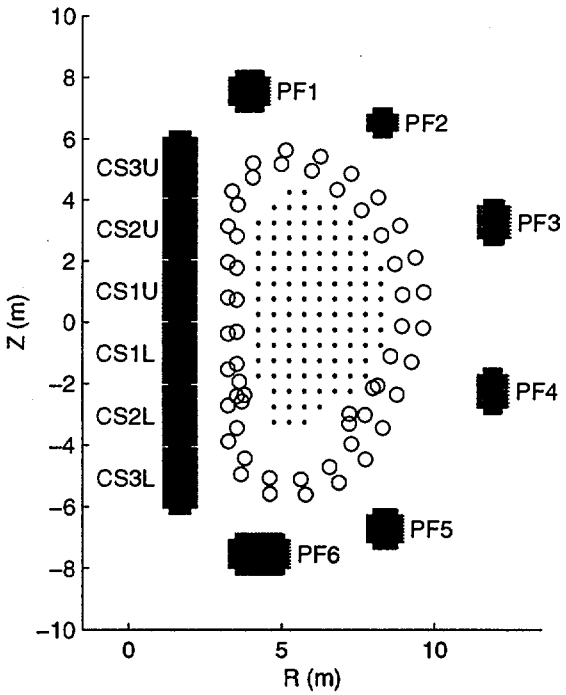

Figure 5: Current loop layout representing the magnetic field sources. Crosses represent the coils, circles the vacuum vessel and dots the plasma.

carry a current defined by the plasma configuration and scaled according to the total plasma current variation.

The field over the cross section of a coil has significant spatial variations. While the field is maximum at the outside, it tends to zero at the center. This requires a certain minimum number of evaluation points for a good representation of the field distribution. In the AC-CRPP Model, a data point is sited at the center of every turn. The field at each point is evaluated as the sum of all contributions from all other turns of all coils, plus the contribution from the vessel and the plasma. The influence of the particular turn itself is neglected, because its influence is small.

2.2.2 Hysteresis Loss Evaluation

A question when evaluating hysteresis loss is the definition of the cycles. In most simulations, the field does not return to its initial value. Fig. 6 (a) shows the evolution of the poloidal magnetic field during a minor disruption of the plasma current. Candidate starting and ending points for cycles are the maxima and the minima of the magnetic field, as well as the starting and

the ending point of the simulation.

If entire cycles have to be defined, a large part of the evolution is not taken into account. In Fig. 6 (a) only the small loop at the beginning is complete, although during the larger, incomplete second cycle losses are also produced. To resolve this, half cycles are defined in the AC-CRPP model, which allow it to cover the whole range of magnetic field change, Fig. 6 (b). The loss is calculated with the same formulas as for entire cycles, but only half of the calculated loss is added.

The second issue with the evaluation of hysteresis loss is how to distribute the loss over the length of the cycle. The formulas only give the loss at the end of a half cycle. To provide a value for the instantaneous hysteresis loss power, the method illustrated in Fig. 6 (c) is proposed. First, the field change with respect to the starting point is evaluated for every time step of the cycle (top, arrows) and the loss energy corresponding to that field change is calculated (middle, dashed lines). The difference between two consecutive loss energy calculations (middle and bottom, solid lines) divided by the time interval gives us the average loss power during a time step (bottom, shaded area).

2.2.3 Coupling Current Loss Evaluation

Equation 10 allows a direct calculation of the coupling loss power during a time step via the field rate of change, approximated by dividing the field difference by the time difference.

When the time scale of the field change is much longer than any of the conductor time constants, steady state conditions can be assumed for the coupling currents. In some cases, with the fastest field changes, the steady state assumption leads to an overestimation of the loss.

2.2.4 Estimated Quantities

The AC-CRPP model provides several output values.

Time evolution of loss power for each coil $P_i(t)$: Contributions of the individual coils to the loss, suited for controller analysis.

Loss power P_i: Average loss power produced during the simulation.

Loss energy Q_i: Loss energy produced during the simulation. If divided by the number of perturbations it is an indicator of how lossy the controller is.

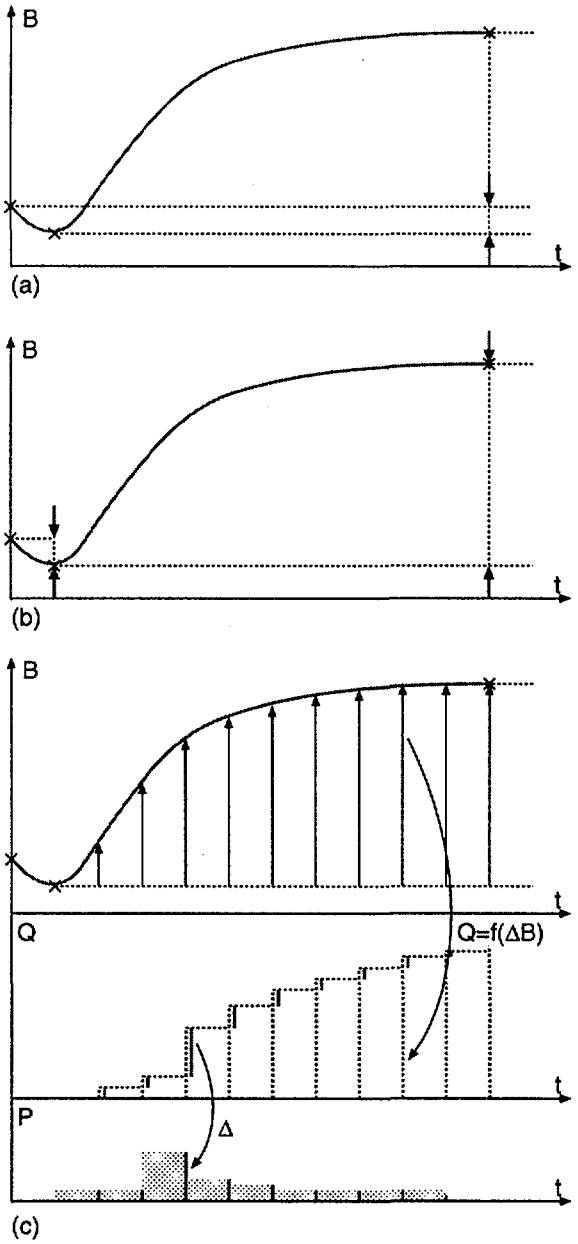

Figure 6: Magnetization loop definition and hysteresis loss evaluation method.

Maximum peak power $\hat{P}_i$: Maximum over all turns of a coil of the peak loss power.

Integral of the square field rate $\int \dot{B}_i^2 \mathrm{d}t$: Measures the control action. The maximum value occurring in a coil over the cross-section is indicated.

All the estimated loss quantities are provided for hysteresis, coupling and total loss.

2.3 Validation

The AC-CRPP model consists of two main parts, the magnetic field calculation and the loss calculation.

The validation of the model was performed in two steps.

2.3.1 Simple Benchmark

First a simple benchmark was performed to check the formulas used in the loss calculation part. A sawtooth waveform for the assumed magnetic field variation, with an amplitude of 0.3 T and a field rate of 0.3 T/s was superimposed on a DC background field of 5 T at a magnet operating temperature of 5 K.

The results from the model agreed with manual calculations with zero difference for the coupling loss and $< 2\%$ difference for the hysteresis loss.

2.3.2 Perturbations during flattop

To check the entire model, ITER simulation data [9] has been used and the results were compared with a complete AC loss model [4]. Two parameters determine an effective internal perturbation to the plasma equilibrium. The internal inductance, l_i, represents the degree of peaking of the plasma current profile and a drop in l_i is frequently observed during plasma perturbations. The plasma pressure normalized to the poloidal field magnetic energy, β_p, frequently drops during a plasma perturbation when kinetic plasma energy is lost. The magnitude and time evolution of l_i and β_p changes generate different types of perturbations for validating the ability of the feedback controller to reject them. Here $l_{i,0}$ and $\beta_{p,0}$ are the nominal values of l_i and β_p.

The three cases of perturbations used are [3]:

- A minor plasma current disruption at the start of burn (MD at SOB) in the ITER scenario is modeled by an instantaneous l_i drop of $0.2(l_{i,0} - 0.5)$ without recovery simultaneous with a β_p drop of 20 % of the equilibrium β_p, followed by 3 s exponential recovery. One Minor Disruption

is considered during the driven burn and two Minor Disruptions are considered during the plasma ramp-up and ramp-down phases. The duration of the simulation is 15 s.

- Compound edge localized modes (CELM) are a feature of tokamak operation in the H-mode and are specified during the sustained burn as an instantaneous l_i drop of $0.06(l_{i,0} - 0.5)$ followed by a 1 s linear recovery simultaneous with a β_p drop of $0.03\beta_{p,0}$ followed by a 0.2 s linear recovery. The repetition time is about 10 s and the simulation lasts 9.99 s.

- Type I edge localized modes (ELM1) also occur during H-mode and are specified during the burn as an instantaneous β_p drop of $0.03\beta_{p,0}$ followed by a 0.1 s linear recovery. They occur with a frequency of 3 Hz and the simulation lasts 9.99 s.

The simulations produce the waveforms of the PF coil current variations, the vessel current variations and the plasma current variations.

The AC-CRPP code first calculates the magnetic field at the centers of the turns. This part is validated by comparing the maximum fields over the cross-section of each coil (Fig. 7), showing good agreement.

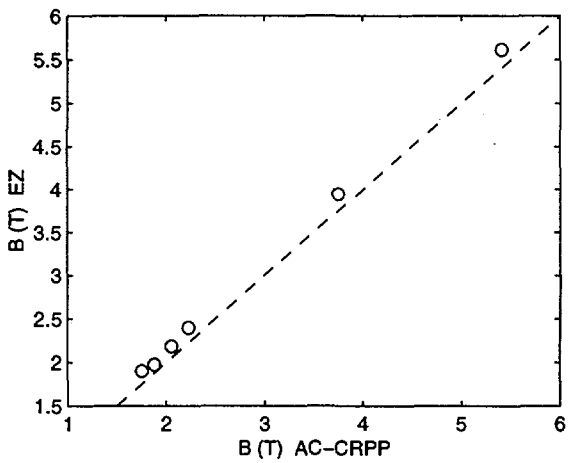

Figure 7: Maximum magnetic field occuring in the cross-section of the six coils calculated by [4] vs. values obtained with the AC-CRPP Model.

From the evolution of the magnetic field, the average AC losses are calculated and compared in Fig. 8. Although there are differences of up to a factor of three, the results can be considered adequate given the general uncertainties in the AC loss modeling. The important feature for studying the

effect of the feedback controller is that smaller losses in the AC-CRPP model correspond to smaller losses in the full model.

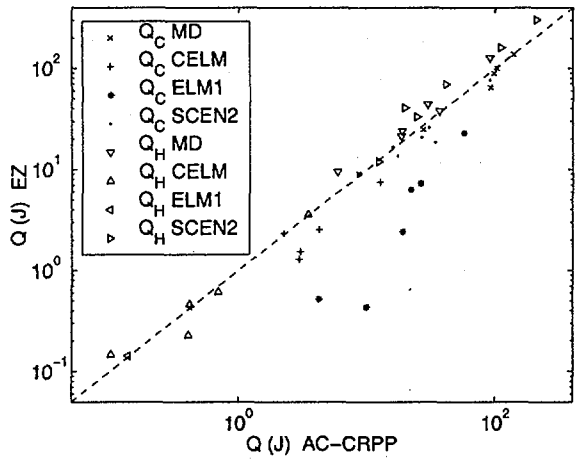

Figure 8: AC loss energy calculated by [4] vs. results from AC-CRPP. Comparison of the six PF coils for the three perturbation types and the entire scenario.

In Fig. 8, the CELM and ELM Type 1 perturbations show a coupling current AC loss overestimation larger than for the Minor Disruption case. This is because CELM and ELM Type 1 provoque fast reactions of the control system and high frequencies are overestimated by the steady-state formula. The agreement is again adequate for studying the feedback controller design.

2.3.3 Simulation of an ITER pulse

The reference ITER pulse has a length of 1800 s with a flattop of 430 s. The AC losses calculated on the basis of the complete plasma discharge were calculated without perturbations, referred to as the scenario loss, averaged over the pulse length to produce a scenario loss power, included in Fig. 8. The scenario losses have the highest hysteresis loss to coupling loss ratio. This is due to the very large field variations during ramp-up and ramp-down and the slow evolution of the scenario.

3 Structure of the Reference Feedback Controller

For the simulations the setup shown in Fig. 9 has been used. The tokamak model is from [1], the perturbation model from [3], the CS and PF coil model from [10] and the controller from [2]. The AC-CRPP model has been evaluated after each completed simulation.

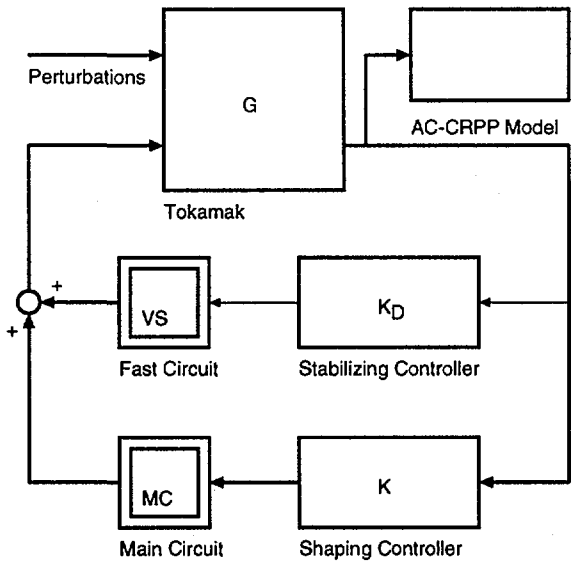

Figure 9: Setup for the simulations

The tokamak is a linearized model and all the variables represent variations with respect to an equilibrium configuration. The power supplies are modeled with first order dynamics plus saturation and delay.

Since the plasma is vertically unstable, the control system must stabilize it. The solution used in the current design is to use one fast power supply for vertical stabilization (VS circuit) connected in series with the slower main converters (MC circuit) used for plasma shaping (see Fig. 10). The fast vertical stabilization system stops the vertical motion and the slower main converter system recovers the displacement.

In the reference controller, the vertical stabilization is achieved by a gain on the vertical speed to control the fast power supply. The plasma current and shape control uses the coil currents, the gaps and the plasma current to control the main power supplies.

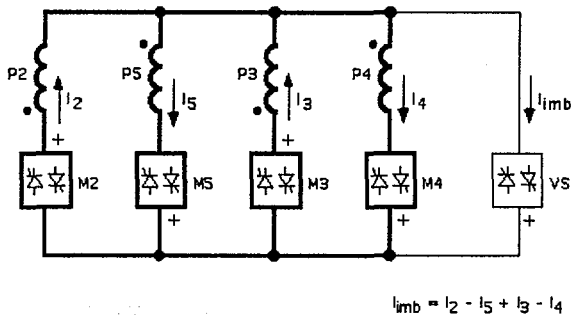

Figure 10: The vertical stabilization circuit is connected to the PF coils 2-5

4 Simulation and Evaluation

The simulations show that the AC loss characteristics depends on the perturbation type. Whereas for the weak but fast ELM type I the coupling current losses dominate, the hysteresis loss is more important for the stronger compound ELM and becomes almost equally important for the minor disruption.

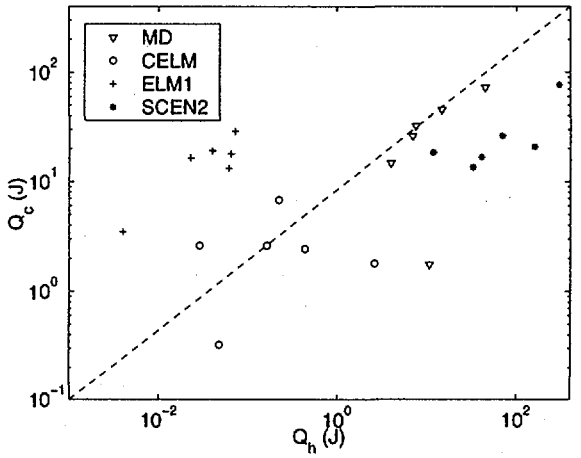

Figure 11: Loss characterization of the six PF coils for different perturbations. The horizontal axis shows the coupling current AC loss and the vertical axis the hysteresis loss. The scenario loss is shown for comparison.

There are two main reasons for a significant difference in the distribution of the AC losses. First, for small amplitude magnetic field changes, the hysteresis loss is small, whereas for larger amplitudes it grows linearly. Second, the small perturbations provoke a stronger reaction by the fast coil system,

which produces high coupling losses, due to its higher bandwidth.

A common feature of all perturbation types is the immediate occurrence of the peak loss which is mainly due to coupling losses, Fig. 12. This peak is caused by the action of the fast stabilizing system to stop the plasma movement. The slower shaping system, which brings the plasma back to its original position does not create high coupling losses because of its lower bandwidth.

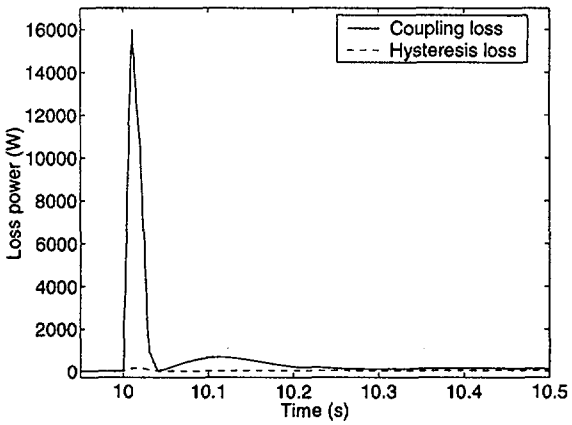

Figure 12: The time evolution of loss power in the case of a CELM perturbation shows a strong peak at the beginning of a perturbation.

The distribution of the losses among the different PF coils shows some important points. PF coils 2 to 5 have high losses due to their use in the fast stabilizing system, whereas the high losses in PF 6 are due to its size and the fact that it is used to fix the divertor configuration. Its coupling loss is relatively small, whereas the hysteresis loss is 5 to 10 times higher than in the other coils. The PF 2 coil has few turns and to compensate this, the controller gain on this coil has to be higher, which leads to coupling losses 5 to 10 times higher than in all other coils (when looking at loss power per unit length).

When looking at an entire shot, the hysteresis losses dominate, Fig. 8, since during ramp-up and ramp-down we have large variations of the magnetic field. To compare the AC losses during the entire scenario with losses from the different perturbations, the following scenario has been assumed:

- A description of the equilibrium currents for $t = [0\,\mathrm{s} : 1800\,\mathrm{s}]$ according to scenario 2 from [11]
- One Minor Disruption during ramp-up

- One Minor Disruption during ramp-down
- A burn of 400 s, with
- One Minor Disruption at the start of burn
- Compound ELMs every 10 s during burn
- ELM type I with a frequency of 3 Hz during burn

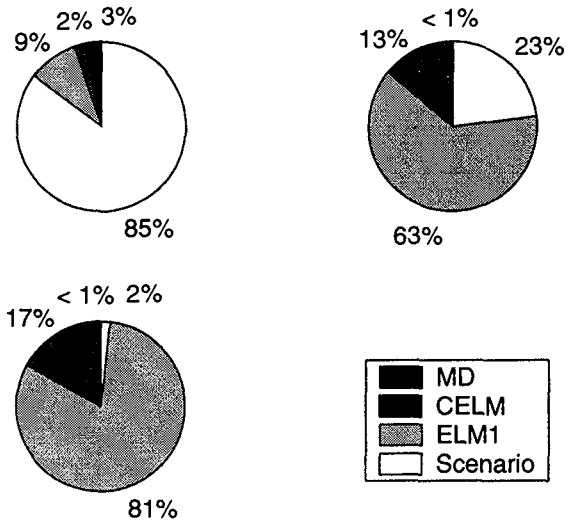

Figure 13: The importance of the irreducible scenario losses decreases with increasing burn durations. Shown are the distributions for 400 s, 10000 s and 172800 s pulses.

Fig. 13 compares the scenario losses with the perturbation losses. The scenario losses dominate for the duration of the ITER pulse (top left) and therefore AC losses of the perturbations are not an issue. The scenario losses, essentially of hysteresis type, can only be reduced by changing the conductor, but not with controller adaptations.

If we assume longer pulse durations with burns of 10000 s and 172800 s (48 hours), the AC losses caused during perturbation rejection become more important and AC loss reduction by controller adjustment becomes interesting (Fig. 13, top right and bottom left).

5 Design of an Improved Controller

The hysteresis losses are proportional to the field variation and the coupling losses increase with the field rate of change. An optimized controller should

therefore try to reduce these two values.

When looking at the output voltages (Fig. 14), we can see that the inner controller produces most of the fast field variations. An examination of the controller influence should therefore focus on this part.

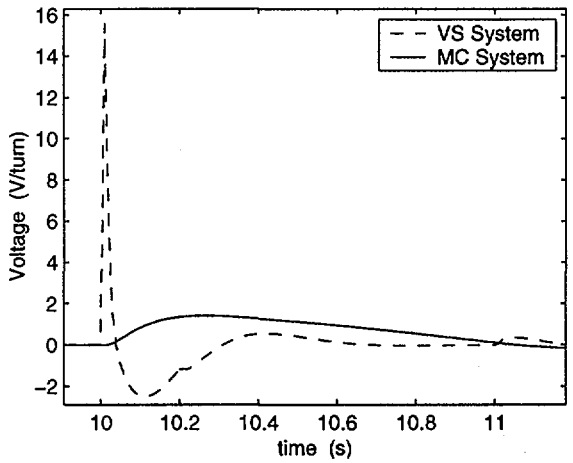

Figure 14: Comparison of the voltages from the VS and MC controllers to drive the PF3 coil in the case of a CELM.

The simplest way to reduce the field rate of change is to reduce the bandwidth of the controller. This would lead to a damping of the high frequency response and therefore reduce the higher frequency magnetic field variations. On the other hand, a fast reacting controller reduces the excursions in the controlled variables, which should reduce the hysteresis loss.

The inner, stabilizing controller is given by:

$$\frac{k_D s}{\tau_i s + 1} = \frac{150\, s}{0.003\, s + 1}. \tag{12}$$

The output voltage of the power supplies is limited, imposing a minimum gain and bandwidth on the controller. The plasma accelerates once it is out of equilibrium and if the controller does not react immediately, it will become too fast to be stopped by the limited voltage (Fig. 15).

When varying the gain of the controller, some interesting observations can be made. The minimum k_D to guarantee stability depends on the perturbation type. While for the type I ELM this minimum gain is around 80, the minor disruption requires a minimum of 100. In the case of a type I ELM, the gain reduction leads to an important reduction of coupling loss, whereas in the case of a minor disruption, the benefit is smaller (see Fig. 18).

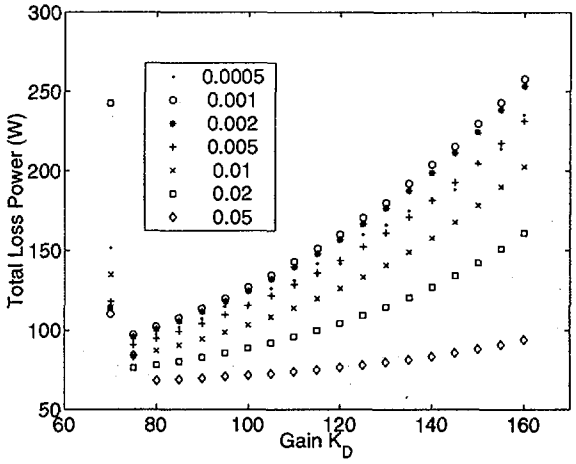

Figure 15: Total loss power as a function of the gain k_d for different time constants τ_i in the case of a type 1 ELM.

If the gain is reduced in order to reduce the AC losses, the three perturbation types have different requirements. The idea used for the design of an improved controller is to adapt the gain to the perturbation type. This requires a real-time estimation of the perturbation amplitude. Perturbations in tokamaks are almost instantaneous and move the system to a state some distance from the equilibrium. By comparing the measured vertical position with the vertical position calculated from the equilibrium PF coil currents we obtain an estimate of this disequilibrium.

The output of such an estimator (Fig. 16) is larger for perturbations requiring a higher gain. The new controller is designed to slide between two different inner controllers, according to the estimator output (Fig. 17). To guarantee a high gain to stop the plasma movement, the maximum value of the estimator output is held for a certain time, 5 s in the tested configuration.

This improved controller considerably reduces the AC losses, especially in the case of the two weaker perturbations, the CELM and ELM1. The performances for the defined perturbations are comparable and the system is stable, but because here even the stronger controller has a lower gain than the original controller, its tolerance to very strong perturbations is reduced. The actual choice of the stronger and weaker controller is a trade-off between stability and performance on one side and AC loss reduction on the other side. As seen in Fig. 15 many possible combinations of time constant and gain exist that have comparable AC losses, but not necesarily the same performance. The best choice depends on the actual tokamak and can only be made once

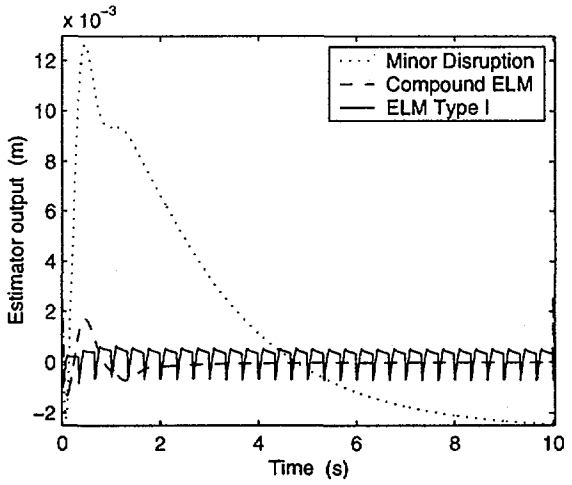

Figure 16: Output of the perturbation estimator for the three perturbation types.

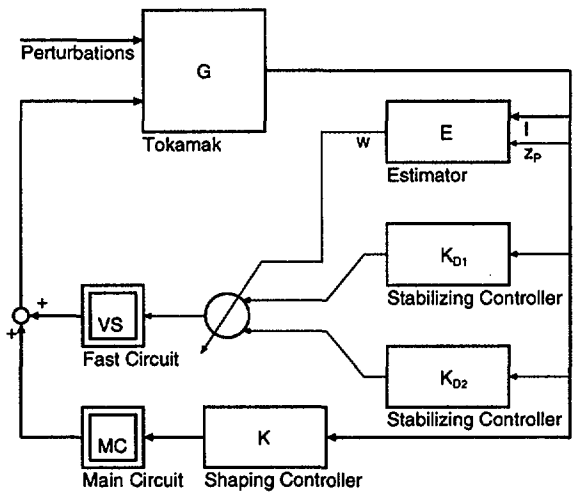

Figure 17: Structure of the AC loss reduced control system.

a model based on the real tokamak has been established.

Although the effect of AC loss reduction may be small compared with other losses, it minimizes heating inside the cable and thus improves conductor stability. Additionally, the importance of this reduction increases with increasing pulse duration, since the inevitable scenario AC losses remain constant, whereas the perturbation AC losses accumulate with the shot duration.

The loss per turn of conductor gives a better idea of how much loss is generated before an exchange of the coolant and allows a comparison of the temperature rise from inlet to outlet (Fig 18). The PF2 coil has a much higher per turn AC loss than the other coils. This is because it has only very few turns and must therefore undergo higher current variations to produce the same effect on the plasma as the other coils, resulting in higher AC losses. To compensate this, the gains of the fast controller can be changed to shift a part of the control action from the PF2 and PF5 coils to the PF3 and PF4 coils. The result is that all the coils have comparable levels of per turn AC losses with the same amount of total AC losses. This would require a change to the turns and current specifications of the coils, since they share a common fast voltage.

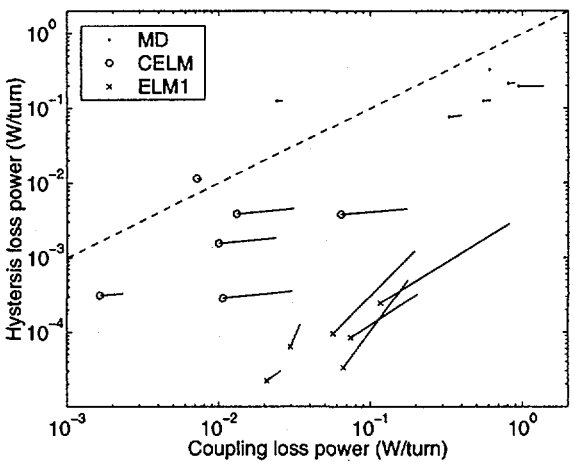

Figure 18: AC loss comparison of the original and improved controller. Starting points show the original values and the end points with the bullets the reduced values.

AC loss reductions similar to those obtained with the proposed scheme can be obtained with a nonlinear control law of the form $ax^3 + bx$ replacing the linear gain of the inner controller. Values of $a = 20000$ and $b = 80$ for a nonlinear gain placed before the lowpass filter showed good results.

6 Discussion and Conclusion

Using existing models of the ITER tokamak and its control system, it has been shown that the AC losses in the superconducting coils can be reduced by adapting the control strategy.

AC losses are due to the reactions of the control system to perturbations of the plasma and noise in the plasma and in the measurement system. Perturbations are almost instantaneous events that move the state of the tokamak away from the equilibrium position. Most of the AC losses occur during and immediately after the perturbation, leading to sharp peaks in the AC loss evolution. Therefore, a significant reduction has to target these peaks, that are mostly due to the fast stabilizing control system.

The need for stability of the plasma position imposes a strong and rapid reaction to strong perturbations. Current control system designs also apply the same strong reactions to weaker perturbations and noise. While this does not influence traditional performance and stability criteria, it causes unnecessary AC losses in the superconducting coils. Weaker controllers allow reductions of the AC losses during weak perturbations to a fifth of their original value.

While the losses due to perturbations can be influenced, the losses due to the ramp-up and ramp-down of the scenario currents cannot be reduced, since they are due to the overall magnetic field changes, which is are defined by the operating scenario.

While the scenario AC losses remain constant, the losses due to perturbations are proportional to the duration of the discharge. Considering a discharge of 1800 s, with a flattop of 430 s the influence of AC loss reduction would be small compared with the total loss. As the discharge becomes longer, the AC loss reduction becomes more significant.

Additionally, the reduction of the peak loss power also improves the transient thermal behavior of the conductor.

The price of the AC loss reduction is a smaller stability margin, but only a slightly reduced performance. Establishing the optimal tradeoff between reducing the AC losses and maximising the stability margin will be made when the true perturbation and noise spectra are measured. This paper proposes a suitable methodology.

Acknowledgements

The authors thank Drs Yuri Gribov and Alfredo Portone for their support in providing the required technical information for the work described in this paper. The work was partly funded by the Fonds National Suisse de la Recherche Scientifique and by EURATOM contract FU05-CT2001-00018 (EFDA/00-551).

References

[1] A. Kavin, ITER-FEAT linear models description, ITER NAKA JWS Issue 1, 10 July 2000

[2] M. Ariola, A. Pironti, A. Portone, A Reduced-Order Controller for Plasma Position and Shape Control in the ITER-FEAT Tokamak, CDC00-REG1452, 3 May 2000

[3] Y. Gribov, Disturbances for Plasma Control Study in ITER-FEAT, ITER NAKA JWS Issue 1, 6 April 2000

[4] E. Zapretilina, Personal Communications, ITER Naka JWS

[5] C.P. Bean, Magnetization of hard superconductors, Phys. Rev. Lett. 8 (1962) 250-253

[6] M. Wilson, Superconducting magnets, Oxford (1983)

[7] A.M. Campbell, A general treatment of losses in multifilamentary superconductors, Cryogenics, 22, 3 (1982)

[8] L. Bottura, A practical fit for the critical surface of NbTi, IEEE Appl. Supercon 10, (2000) 1054

[9] Y. Gribov, Personal Communications, ITER Naka JWS

[10] Y. Gribov, ITER-FEAT CS and PF coils for PF Control Study, ITER NAKA JWS Issue 2, 7 April 2000

[11] Y. Gribov, Plasma Operation Scenarios, ITER NAKA JWS Issue 3, 24 March 2000

AC-CRPP User Manual

Beat Schärz[a] Pierluigi Bruzzone[b] Jean-Yves Favez[c]
Jonathan B. Lister*,[a] Elena Zapretilina[d]

November 22, 2001

*Corresponding author. Tel.: +41-21-693-3405; Fax.: +41-21-693-5176; E-mail: jo.lister@epfl.ch
[a]EPFL-CRPP, 1015 Lausanne, Switzerland
[b]EPFL-CRPP Fusion Technology, 5232 Villigen-PSI, Switzerland
[c]EPFL-DGM-IA, 1015 Lausanne, Switzerland
[d]Efremov Institute, St. Petersburg, Russian Federation

Abstract

This documents describes the use of the AC-CRPP AC Loss evaluation code.

1 Introduction

AC-CRPP code provide a fast way to estimate the magnitude of AC losses inside superconducting NbTi coils of future tokamaks. The purpose of the code is a rough estimation of the losses, to get an idea of the performance of a certain plasma position and shape controller with respect to AC losses.

The model contains some simplifications, that considerably reduce the computing time, but have only limited influence on the precision of the result. This because a precise AC loss calculation is not yet possible and a precision better than an order of magnitude cannot be expected.

AC loss calculation requires the knowledge of the magnetic field evolution and therefore of the currents flowing inside the tokamak. The most important contributions come from the coils and the plasma. The model allows, to further include the passive vessel structure.

Since the spatial distribution of the magnetic field inside the coils has important variations, the magnetic field is evaluated at different points (turns) of the coils that correspond to the windings.

The AC-CRPP code is splitted into two parts, the `field_coeff.m` and the `losseval.m` routine. The main part, `losseval.m`, uses several `.mat` files stored in the `data` subdirectory to calculate the AC-Losses. Since one step of the preparations, the calculation of some machine geometry dependent coefficients, is relatively time consuming and remains constant for a given machine, it has been put into a separate file, `field_coeff.m`, that needs to be executed only once per tokamak.

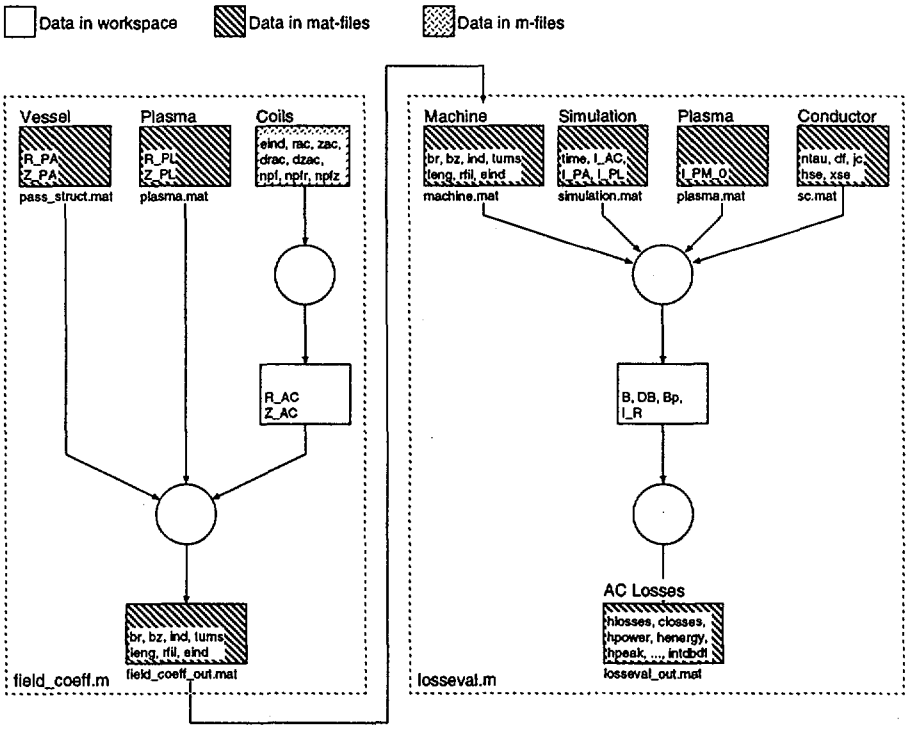

Figure 1: Chart of the data flow inside the AC-CRPP code.

In Fig. 1 the basic structure of the AC-CRPP code is illustrated, with the two `.m` files as well as the `.mat` files used to input data.

The tokamak is modeled as a set of current carrying loops. The loops are centered around the y-axis and defined by their intersection with the right half of the xy-plane. Currents have to be provided for each coil and for each section of the vessel plus one for the plasma.

2 field_coeff.m

The input data for the field_coeff.m routine is located in the plasma.mat and pass_struct.mat files and in the top section of the code.

The geometry of the coils has to be defined at the top of the field_coeff.m file:

rac, {m}: a-by-1 matrix containing the horizontal positions of the coil centers.

zac, {m}: a-by-1 matrix containing the vertical positions of the coil centers.

drac, {m}: a-by-1 matrix containing the widths of the coils.

drac, {m}: a-by-1 matrix containing the heights of the coils.

npf, {turns}: a-by-1 matrix containing the number of turns per coil.

npfr, {turns}: a-by-1 matrix containing the number of turns of a coil in horizontal direction.

npfz, {turns}: a-by-1 matrix containing the number of turns of a coil in vertical direction.

eind, {-}: b-by-1 matrix containing the numbers of the coils for which the magnetic field should be calculated.

The turns are arranged in npfr columns and npfz lines over the area defined by drac and dzac (Fig. 2). If the number of turns in a coil is not equal to the product of npfr and npfz, the number of turns in the rightmost column is adapted. Best results are obtained if for the last column the same or a slightly smaller number of columns remains.

If the file pass_struct.mat exists within the search path, the c-by-1 arrays R_PA {m} and Z_PA {m} are loaded from it and used to define the horizontal and vertical positions of a set of conductor loops that model the passive structure of the tokamak. Else, the passive structure is not taken into account.

If the file plasma.mat exists within the search path, the d-by-1 arrays R_PL {m} and Z_PL {m} are loaded from it and used to define the horizontal and vertical positions of a grid of conductor loops that model the plasma. The simulation data has to provide only one plasma current, but this one will be distributed according to I_PM_0 {A} in plasma.mat to get a better representation of the magnetic field caused by the plasma. Else, the plasma is modelled by one conductor at the position specified by the variables R_PL

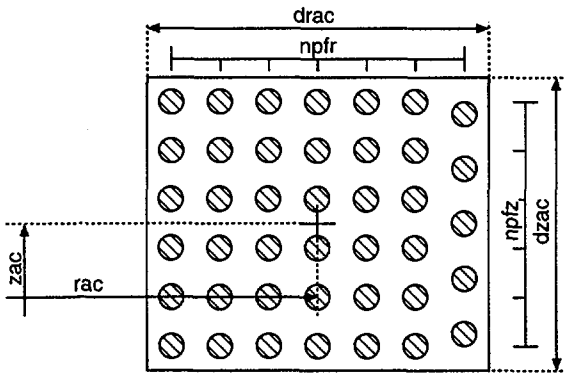

Figure 2: Coil layout.

and Z_PL in the file `field_coeff.m`. It is also possible to ignore the influence of the plasma. In this case, the file `plasma.mat` should not exist within the search path and the variables R_PL and Z_PL should be defined as empty arrays.

The main purpose of the function `field_coeff.m` is to calculate the two g-by-$(a+c+d)$ matrices $\boldsymbol{b^r}$ and $\boldsymbol{b^z}$ linking the currents to the magnetic field.

$$B_i = \sqrt{\Big(\sum_j b^r_{ij}\, I_j\Big)^2 + \Big(\sum_j b^z_{ij}\, I_j\Big)^2}$$

The components of the vector $\vec{I}$ are the coil, vessel and plasma currents and the components of the vector $\vec{B}$ are the magnetic fields at the center of the g turns of the analysed coils.

The coefficients are defined by

$$b^r_{ij} = \frac{\mu_0 h}{2\pi r_i \sqrt{(r_i+r_j)^2+(z_i-z_j)^2}}\left(-K_{ij} + \frac{r_i^2+r_j^2+(z_i-z_j)^2}{(r_i-r_j)^2+(z_i-z_j)^2}E_{ij}\right)$$

$$b^z_{ij} = \frac{\mu_0}{2\pi r_i \sqrt{(r_i+r_j)^2+(z_i-z_j)^2}}\left(K_{ij} + \frac{r_i^2-r_j^2-(z_i-z_j)^2}{(r_i-r_j)^2+(z_i-z_j)^2}E_{ij}\right)$$

where K_{ij} and E_{ij} are elliptic integrals of the first and second kind respectively.

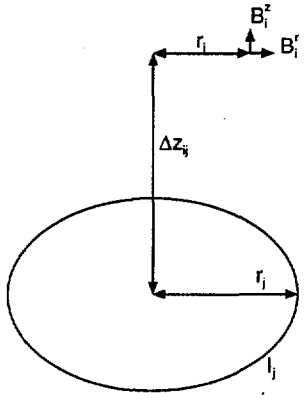

Figure 3: Conductor layout.

$$
\begin{aligned}
K_{ij}(k, 2\pi) &= \int_0^{2\pi} \frac{\mathrm{d}t}{\sqrt{1 - k_{ij}^2 \sin^2 t}} \\
&= \frac{\pi}{2}\left(1 + \frac{1}{4}k_{ij}^2 + \frac{9}{64}k_{ij}^4 + \left(\frac{(2m)!}{2^{2m}(m!)^2}\right)^2 k_{ij}^{2m} + \dots\right) \\
E_{ij}(k, 2\pi) &= \frac{1}{4}\int_0^{2\pi} \sqrt{1 - k_{ij}^2 \sin^2 t}\, \mathrm{d}t \\
&= \frac{\pi}{2}\left(1 - \frac{1}{4}k_{ij}^2 - \frac{3}{64}k_{ij}^4 - \left(\frac{(2m)!}{2^{2m}(m!)^2}\right)^2 \frac{k_{ij}^{2m}}{2m-1} - \dots\right)
\end{aligned}
$$

and k_{ij} is defined by

$$k_{ij}^2 = \frac{4 r_i r_j}{(r_i + r_j)^2 + (z_i - z_j)^2}.$$

Additionally, the routine creates a g-by-1 vector **rfil** with the radii of the turns of the analysed coils, a a-by-1 vector **turns** with the number of turns of all coils, a b-by-1 vector **eind** with the numbers of the analysed coils, a b-by-1 vector **leng** {m} with the conductor length of the evaluated coils, a bw-by-g matrix **ind** to transform from indices based on the turns to indices based on the evaluated coils,

$$ind_{ij} = \begin{cases} 1 & \text{if turn } j \text{ belongs to coil } i \\ 0 & \text{else} \end{cases}$$

with i spanning over all the coils defined in the variable `eind` and j spanning over all the turns of the coils defined in the variable `eind`.

The `.mat` files should be in a subirectory called `data` and the result will be saved in `data/field_coeff_out.mat`.

3 losseval.m

The routine losseval.m evaluates the magnetic field and calculates the AC losses. Fig. 4 shows its structure and the flow of data within the code. Input data comes from five .mat files.

3.1 machine.mat

The file machine.mat is the same as the file field_coeff_out.mat. It contains the coefficients calculated from the geometrical description of the tokamak.

3.2 scenario.mat

Coil scenario current, I_AC_0, **{A}:** a-by-1 matrix describing offset values that will be added to the coil current evolutions.

Vessel scenario current, I_PA_0, **{A}:** c-by-1 matrix describing offset values that will be added to the vessel current evolutions. This values are usually zero.

Plasma scenario current, I_PL_0, **{A}:** Scalar value describing an offset value that will be added to the plasma current evolution.

3.3 plasma.mat

Plasma current distribution, I_PM_0, **{A}:** d-by-1 matrix describing the distribution of the total plasma current on the different conducting loops that model the plasma. The values will be scaled such that their sum is equal to the sum of I_PL_0 and I_PL.

3.4 simulation.mat

Time, time, **{s}:** e-by-1 matrix stored in workspace with the absolute values of the time in seconds. Uneven time steps are possible.

Coil current variations, I_AC, **{A}:** e-by-a matrix describing the variations of the currents in the m coils from the scenario currents I_AC_0 specified in scenario.mat.

Passive current variations, I_PA, **{A}:** e-by-c matrix describing the variations of the p passive currents from the scenario currents I_PA_0 specified in scenario.mat.

Plasma current variations, I_PL, {A}: e-by-1 matrix describing the variations of the plasma current from the scenario current I_PL_0.

3.5 sc.mat

Average decay constant, ntau, {s}: b-by-1 matrix describing the behavior of the cable for coupling loss calculations. This value has to be measured on real cables.

Superconducting filament diameter, df, {m}: b-by-1 matrix used for hysteresis loss calculation.

Critical current density, jc, {A/m2}: f-by-2 matrix describing the dependence of the critical current density j_c of the applied magnetic field. The first column contains the magnetic field in T and the second the critical current density in Aperm2. The code interpolates the real value from this table. It should span the whole range of possible magnetic fields. Outside the defined range, linear approximation is applied.

Superconducting cross-section, hse, {m2}: b-by-1 matrix used to convert from specific to absolute hysteresis loss power.

Total cross-section, hse, {m2}: b-by-1 matrix used to convert from specific to absolute coupling loss power.

3.6 Formulae: Descriptions and Assumptions

The total plasma current is the sum of I_PL_0 and I_PL. This current is distributed proportional to the description in I_PM_0 according to

$$\begin{aligned} I_{PM}(t) &= I_{PL}(t)\frac{I_{PM,0}}{\sum I_{PM,0}} \\ I_{PM,0} &= I_{PL,0}\frac{I_{PM,0}}{\sum I_{PM,0}} \end{aligned} \tag{1}$$

where I_PM describes the current evolution inside the conductor loops that model the plasma.

The absolute current evolutions are the sum of the scenario (or offset) values and the relative current evolutions

$$I(t) = [I_{AC,0}\, I_{PA,0}\, I_{PM,0}] + [I_{AC}(t)\, I_{PA}(t)\, I_{PM}(t)]. \tag{2}$$

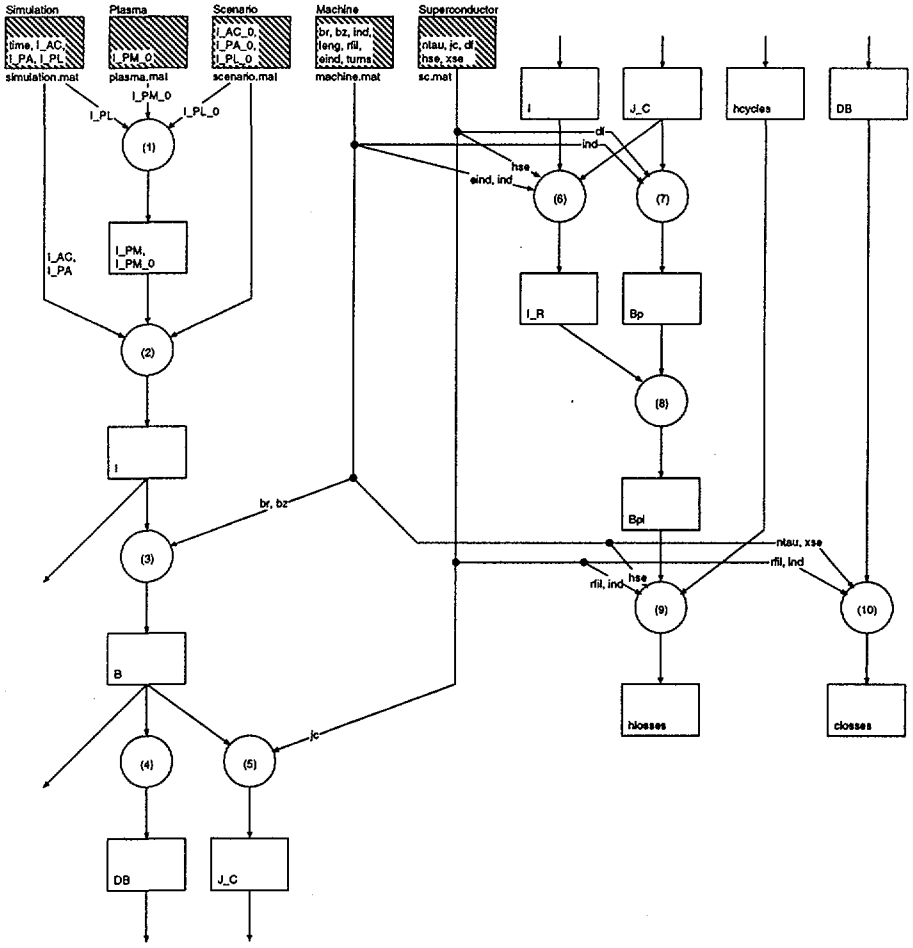

Figure 4: Dataflow.

The components of the magnetic field depend linearly on the currents

$$B(t_i) = \sqrt{B_r(t_i)^2 + B_z(t_i)^2} = \sqrt{(br\, I(t_i))^2 + (bz\, I(t_i))^2} \tag{3}$$

where br and bz denotes the matrix of coefficients calculated by `field_coeff.m` and $I(t)$ the time dependent vector whose components are the currents.

The field rate is approximated by

$$\dot{B}(t_i) \approx \frac{DB(t_i)}{dtime(t_i)} = \frac{B(t_i) - B(t_{i-1})}{t_i - t_{i-1}} \tag{4}$$

The critical current density J_C is interpolated linearly from a table j_c and the magnetic field evolution $B(t_i)$.

$$J_C(t_i) = j_c(B(t_i)) \tag{5}$$

The ratio between applied and critical current I_R

$$I_R(t_i) = \frac{I(t_i)}{J_C(t_i) hse} \tag{6}$$

The penetration field B_p is assumed obey Bean's law [1]. It is calculated for every turn and time step individually.

$$B_p(t_i) = \frac{\mu_0 d_f}{\pi} J_C(t_i) \tag{7}$$

In the case of an applied longitudinal transport current, the value obtained for B_p has to be corrected to B_p^I

$$B_p^I(t_i) = B_p(t_i)(1 - I_R(t_i)) \tag{8}$$

The hysteresis loss calculation has to distinguish between small and large field changes. The hysteresis loss formula uses the magnitude of a cycle as main input. To specify to loss between two succeeding time steps, half cycles are introduced [2]. The field change therefore refers to the beginning of the simulation or to the last field reversal, whichever is closer in time. The additional loss is the difference in total loss to the preceding time step.

$$q_{h,turn}(\Delta B) = \begin{cases} \frac{1}{2}\frac{\Delta B^3}{3\mu_0 B_p}\left(1 - \frac{\Delta B}{4B_p}\right) & \text{if } \Delta B < 2B_p \\ \frac{1}{2}\frac{4\Delta B B_p}{3\mu_0}\left(1 - \frac{B_p}{\Delta B}\right) & \text{if } \Delta B \geq 2B_p \end{cases}$$

$$Q_{h,turn}(\Delta B) = 2\,\pi\, r_{fil}\, hse\, q_{h,turn}(\Delta B)$$

$$Q_{h,coil}(\Delta B) = ind\, Q_{h,turn}(\Delta B) \tag{9}$$

The coupling loss calculation assumes steady-state conditions (i.e. the duration of a field change is longer than any conductor time constant). The coupling loss in a turn is

$$q_c(t_i) = \frac{n\tau}{\mu_0}\dot{B}^2(t)$$

$$Q_c(t_i) = 2\,\pi\, r_{fil}\, xse\, q_c(t_i)$$

$$\dot{B}^2 \approx \left(\frac{\Delta B}{\Delta t}\right)^2$$

and the sum in a coil is obtained by

$$Q_{c,coil} = ind\, Q_{c,turn} \tag{10}$$

3.7 Results

The results of the `losseval.m` routine are stored in `data/losseval_out.mat` and in the workspace. The available variables are:

```
>> whos
  Name          Size          Bytes  Class

  cenergy          6x1             48  double array
  closses       1000x1351     10808000  double array
  cpeak            6x1             48  double array
  cpower           6x1             48  double array
  henergy          6x1             48  double array
  hlosses       1000x1351     10808000  double array
  hpeak            6x1             48  double array
  hpower           6x1             48  double array
  intdbdt       1351x1           10808  double array
  tenergy          6x1             48  double array
  tpeak            6x1             48  double array
  tpower           6x1             48  double array

Grand total is 2703405 elements using
 21627240 bytes
```

The following variables all exist with one of the prefixes, `h` for hysteresis loss, `c` for coupling current loss and `t` for total loss, being the sum of hysteresis and coupling current loss.

Loss energy, `energy`, {J/coil} b-by-1 matrix containing the loss energy dissipated per coil during the simulation.

Average loss power, `power`, {W/coils} b-by-1 matrix containing the average loss power dissipated per coil during the simulation.

Peak loss power, `peak`, {W/turn} g-by-1 matrix containing the maximum over all turns of a coil of the loss power occuring during a simulation.

Loss evolution, `losses`, {J/turn} $(e-1)$-by-g matrix containing the loss energy dissipated in a turn between two succeding time steps.

Additionally, the variable `intdbdt` is provided. This is the integral over time of the square field rate of change. The value is provided for each turn individually and gives a good idea of the control action achieved on the plasma.

References

[1] C.P. Bean, Magnetization of hard superconductors, Phys. Rev. Lett. 8 (1962) 250-253

[2] B. Schärz, P. Bruzzone, J.Y. Favez, J.B. Lister, E. Zapretilina, The Effect of Feedback Control on Superconducting Tokamak AC Losses, Submitted for publication

[3] Y. Gribov, Plasma Operation Scenarios, ITER NAKA JWS Issue 3, 24 March 2000

A Example

The code comes with some example `.mat` files. These can be found in the `data` subdirectory.

`pass_struct_ITERFEAT.mat` contains a description of the passive structure of the ITER-FEAT tokamak.

`machine_ITERFEAT.mat` is a description of the ITER-FEAT tokamak geometry. This file is the result of `losseval.m`.

`scenario_zero.mat` contains the offset values for the currents of ITER-FEAT if all these values are zero.

`scenario_SOB.mat` contains the offset values for the currents of ITER-FEAT according to scenario 2, SOB.

`scenario_SOF.mat` contains the offset values for the currents of ITER-FEAT according to scenario 2, SOF.

`plasma_ITERFEAT.mat` contains a description of a plasma for ITER-FEAT.

`sc_ITERFEAT.mat` contains a description of the superconducting cables used in the PF coils of ITER-FEAT.

`simulation_total.mat` contains a description of scenario 2 of ITER-FEAT.

`simulation_md.mat` contains a simulation of a minor disruption.

`simulation_celm.mat` contains a simulation of a compound ELM.

A.1 Case 1: Simulation without offset

The first case is an examination of the scenario 2 defined for ITER-FEAT in [3]. The file `simulation_total.mat` contains a description of the current evolutions and is copied to `simulation.mat`. THe other files used are `machine_ITERFEAT.mat`, `scenario_zero.mat`, `plasma_ITERFEAT.mat` and `sc_ITERFEAT.mat`. These are copied to `machine.mat`, `scenario.mat`, `plasma.mat` and `sc.mat`. The zero scenario file is used because the data in the simulation file already contains absolute currents.

Once these preparations done, the routine `losseval.m` is called at the Matlab prompt.

```
>> losseval

Machine description loaded
Scenario description loaded
Plasma description loaded
Superconductor description loaded
Simulation description loaded
Time elapsed:  0.57638 s

Executed correction.m
Time elapsed:  0.64104 s

Magnetic field evolutions calculated
Coil current between 45020.0803 A and 0 A
 resp. -44672.8972 A
Passive current between 0 A and 0 A
 resp. 0 A
Plasma current between 15000000 A and 0 A
Magnetic field between 5.4143 T and 0 T
Time elapsed:  0.80114 s

Hysteresis losses calculated
Time elapsed:  1.0858 s

Coupling losses calculated
Time elapsed:  1.1172 s

Total losses calculated
Time elapsed:  1.1335 s
```

The results can either be consulted in the file `losseval_out.mat` or in workspace:

```
>> whos
  Name          Size          Bytes  Class

  cenergy       6x1              48  double array
  closses      30x1351       324240  double array
  cpeak         6x1              48  double array
  cpower        6x1              48  double array
  henergy       6x1              48  double array
  hlosses      30x1351       324240  double array
  hpeak         6x1              48  double array
  hpower        6x1              48  double array
```

```
  intdbdt     1351x1          10808  double array
  tenergy        6x1             48  double array
  tpeak          6x1             48  double array
  tpower         6x1             48  double array

Grand total is 82465 elements using 659720 bytes
```

The AC loss energy (J) for the entire scenario 2 for the six PF-Coils is:

```
>> henergy

henergy =

   1.0e+05 *

    1.8613
    0.1177
    0.3661
    0.3093
    0.6173
    3.2399

>> cenergy

cenergy =

   1.0e+04 *

    2.0739
    1.8388
    1.6683
    1.3478
    2.6184
    7.6579
```

A.2 Case 2: Simulation with offset

If we want to use simulation data from the linearised Simulink model, we have to add the scenario currents to the current variations. Therefore the file `scenario_SOB.mat` is copied to `scenario.mat` and the file `simulation_celm.mat` to `simulation.mat`.

```
>> losseval
```

```
Machine description loaded
Scenario description loaded
Plasma description loaded
Superconductor description loaded
Simulation description loaded
Time elapsed:  0.13393 s

Executed correction.m
Time elapsed:  0.20046 s

Magnetic field evolutions calculated
Coil current between 40577.7288 A and
 721.5501 A resp. -37584.3735 A
Passive current between 156718.9485 A
 and 160.8063 A
 resp. -132400.0481 A
Plasma current between 15133125 A and
 14976142.0124 A
Magnetic field between 5.3119 T and 0.051999 T
Time elapsed:  6.7076 s

Hysteresis losses calculated
Time elapsed:  34.9867 s

Coupling losses calculated
Time elapsed:  37.2009 s

Total losses calculated
Time elapsed:  37.817 s
```

The AC loss energy (J) for the compound ELM for the six PF-Coils is:

```
>> henergy

henergy =

    0.6990
    3.6709
    2.6944
    0.4206
    8.7057
   45.0587

>> cenergy
```

```
cenergy =

    5.5211
  175.9949
   42.3986
   48.9943
   64.5550
   30.8718
```

A.3 Case 3: Simulation without offset

In the third case, the plasma current falls to zero within 20 ms, while all other currents remain at their values. For this case, the file `simulation_dis.mat` is copied to `simulation.mat` and `scenario_zero.mat` to `scenario.mat`.

```
>> losseval

Machine description loaded
Scenario description loaded
Plasma description loaded
Superconductor description loaded
Simulation description loaded
Time elapsed:  3.1141 s

Executed correction.m
Time elapsed:  3.1935 s

Magnetic field evolutions calculated
Coil current between 40470.5882 A and
 747.6636 A resp. -37570.0935 A
Passive current between 0 A and 0 A resp. 0 A
Plasma current between 15000000 A and 0 A
Magnetic field between 5.297 T and 0.044228 T
Time elapsed:  7.3477 s

Hysteresis losses calculated
Time elapsed:  19.0664 s

Coupling losses calculated
Time elapsed:  20.5031 s

Total losses calculated
```

```
Time elapsed:  21.1206 s
```

The AC loss energy (J) is

```
>> henergy

henergy =

   1.0e+03 *

    2.7881
    0.3403
    0.2649
    0.3081
    0.5325
    1.7543

>> cenergy

cenergy =

   1.0e+05 *

    5.8202
    1.5801
    1.1833
    1.0979
    2.1707
    6.0714
```